Graphene field effect transistors for in vitro and ex vivo recordings

D. Kireev, I. Zadorozhnyi, T. Qiu, D. Sarik, F. Brings, T. Wu, S. Seyock, V. Maybeck, M. Lottner, B. M. Blaschke, J. Garrido, X. Xie, S. Vitusevich, B. Wolfrum, A. Offenhäusser

Recording extracellular potentials from electrogenic cells (especially neurons) is the hallmark destination of modern bioelectronics. While fabrication of flexible and biocompatible *in vivo* devices via silicon technology is complicated and time-consuming, graphene field-effect transistors (GFETs), instead, can easily be fabricated on flexible and biocompatible substrates. In this work, we compare GFETs fabricated on rigid (SiO_2/Si and sapphire) and flexible (polyimide) substrates. The GFETs, fabricated on the polyimide exhibit extremely large transconductance values, up to 11 $mS \cdot V^{-1}$, and mobility over 1750 $cm^2 \cdot V^{-1} \cdot s^{-1}$. *In vitro* recordings from cardiomyocyte-like cell culture are performed by GFETs on a rigid transparent substrate (sapphire). Via multichannel measurement we are able to record and analyze both: difference in action potentials as well as their spatial propagation over the chip. Furthermore, the controllably flexible polyimide-on-steel (PIonS) substrates are able to *ex vivo* record electrical signals from primary embryonic rat heart tissue. Considering the flexibility of PIonS chips, together with the excellent sensitivity, we open up a new road into graphene-based *in vivo* biosensing.

***Index Terms* — Graphene, GFETs, solution gating, *in vitro* biosensor, *ex vivo* biosensor, bioelectronics, electrophysiology**

I. Introduction

Silicon-based solid-state devices, especially the ones based on CMOS technology, are great for sensing applications [1], [2]. Such devices have plenty of advantages, coming from over sixty years of extensive research [3]. However, the requirement of flexibility and long-term biocompatibility is a difficult to achieve feature for the Si-based sensors [4]. The stiffness of silicon is the main disadvantage, which leads to inflammation, glia and tissue response to the implanted silicon-based probes [5]. It is, of course possible to thin down the silicon and transfer the devices into a flexible substrate, but such technology is very complicated. Therefore it is important to bring the solid-state advantages into flexible and biocompatible shell. The most interesting and promising material in this regard is graphene [6]. Known for its outstanding electrical properties, graphene is the supreme material for such a purpose [7]. Moreover, biocompatibility and cytocompatibility of a large area monolayer graphene on a substrate has been proven [8], [9] and even cells grown on bare graphene preserve their electrical behavior [10].

As discussed elsewhere [11], the graphene, biased via a liquid, exhibits a very impressive gating behavior. The change of reference electrode potential from zero to 500 mV is usually enough to move from p-type to n-type regime through the Dirac point. At the same time, the conductivity curve is very steep and the resulting transconductance, $g_{max} = \Delta I_{DS}/\Delta V_{GS}$, can reach 11 $mS \cdot V^{-1}$, corresponding to area-normalized transconductance of 1.65 $mS \cdot V^{-1} \cdot \square$ (device's W=20 µm, L=3 µm).

In this work, the graphene field effect transistors (GFETs) are fabricated on different substrates: SiO_2/Si, Sapphire and controllably flexible polyimide-on-steel (PIonS). Polyimide (PI), a flexible and biocompatible polymer, is being widely used as a substrate in biosensing applications due to its great properties. The robust structure, chemical, mechanical and biological stability [12], and absence of dangling bonds make it a great substrate for interfacing with graphene. Our analysis, showing that the PIonS based GFETs exhibit the best performance, compared to SiO_2/Si and sapphire only proves the fact. However, transconductance is not the only dominant factor: one has to take into account the noise values. Our findings show that sapphire-based devices exhibit lower noise values than polyimide. Transparency of the sapphire, combined with low noise performance allows us to measure cardiac HL-1 cells' action potentials. With the flexible devices we measured potentials *ex vivo* from heart tissue as a step towards *in vivo* experiments.

This paragraph of the first footnote will contain the date on which you submitted your paper for review. The work was supported by Helmholtz-CAS JRG funding. B. M. Blaschke, M. Lottner, and J. Garrido also would like to acknowledge funding from the Graphene Flagship (Contract No. 604391).

D. Kireev, I. Zadorozhnyi, T. Qiu, D. Sarik, F. Brings, S. Seyock, V. Maybeck, S. Vitusevich, and A. Offenhäusser are with the Institute of Bioelectronics (ICS-8/PGI-8), Forschungszentrum Jülich, 52425 Jülich, Germany (e-mail: d.kireev@fz-juelich.de; i.zadorozhnyi@fz-juelich.de; t.qiu@fz-juelich.de; d.sarik@fz-juelich.de; f.brings@fz-juelich.de; s.seyock@fz-juelich.de>; v.maybeck@fz-juelich.de; a.offenhaeusser@fz-juelich.de).

T. Wu and X. Xie are with State Key Laboratory of Functional Materials for Informatics, Shanghai Institute of Microsystem and Information Technology, Chinese Academy of Sciences, 865 Changning Road, Shanghai 200050 China (e-mail: trwu@mail.sim.ac.cn; xmxie@mail.sim.ac.cn).

M. Lottner and B. M. Blaschke are with Walter Schottky Institut, Technische Universität München, Am Coulombwall 4, 85748 Garching, Germany (e-mail: martin.lottner@wsi.tum.de; Benno.Blaschke@wsi.tum.de).

J. Garrido was with with Walter Schottky Institut, TUM, Am Coulombwall 4, 85748 Garching, Germany. He is now with Catalan Institute of Nanoscience and Nanotechnology (ICN2), Campus UAB – Edifici ICN2, 08193 Bellaterra (Barcelona) Spain (e-mail: joseantonio.garrido@icn.cat).

B. Wolfrum was with Institute of Bioelectronics (PGI-8/ICS-8), Forschungszentrum Jülich, 52425 Jülich, Germany. He is now with Neuroelectronics, Technische Universität München – IMETUM, Boltzmannstraße 11, 85748 Garching, Germany (email: bernhard.wolfrum@tum.de).

II. Materials and methods

A. Fabrication and design

We fabricate the devices on three kinds of substrates: polyimide-on-steel, SiO_2/Si, and sapphire. The PIonS substrates are fabricated by spin-coating two thick layers of polyimide (PI 2611, HD Microsystems) on top of a steel substrate, followed by baking at 350ºC for complete imidization. The double PI layer is required to reduce the surface roughness. The final PI thickness is approximately 10 µm.

Graphene is grown via chemical vapor deposition (CVD) on 25 µm thick copper foils in an $Ar/H_2/CH_4$ gas mixture (300 sccm, 15 sccm and 0.5-1.0 sccm respectively). During the growth process, of 30 minutes long, the temperature is set to approximately 1050-1070 ºC [13]. The grown graphene is mostly a monolayer, as studied via Raman and optical methods, as shown in Wu et al. [13]. Afterwards, a thin layer (300-500nm) of poly(methyl methacrylate) (PMMA) spin-coated on top of the copper foil is used as a support for further transfer [14]. The PMMA/graphene stack was then transferred on top of the substrates with pre-fabricated Au/Ti markers for further alignment. After annealing at 160ºC for 5 minutes, the PMMA is removed in warm acetone (45ºC) and the substrate is cleaned in isopropanol (IPA). Next, the graphene is patterned and contacted using standard UV-photolithography (AZ5214 photoresist, and oxygen plasma for patterning; nLOF/LOR for Au/Ti metallization, and HD 8820 for passivation).

The array design on SiO_2/Si and on PIonS substrates have exactly the same geometry, topography, and the fabrication flow described above. They consist of a 32 transistor array with individual pairs of sources and drains. In contrast, the sapphire chips have a different design: 64 drains and one common source electrode. The graphene is also CVD grown, but from a different source [15]. The fabrication flow is also slightly different: the graphene is transferred on top of already evaporated metallization, then defined by oxygen plasma and metallized again [15], [16]. In this way, graphene is contacted from both sides. Passivation is done by photostructurable SU-8 photoresist.

B. Cell culture

The HL-1 cell culture line is received in a frozen state [17]. The cells are thawed and cultured in a T25 flask for several days until they reach 100% surface coverage. The confluent layer is then electrically active and beating with frequency of 1-5 Hz [18]. Prior to culturing the cells on a chip, a glass ring is mounted to the chip to form a culture container and the surface of the chip is coated with fibronectin (5 µg/mL) solved in gelatin (0.2 µg/mL) for improved cellular adhesion. The cardiomyocytes are split, and approximately 5×10^4 cells are placed inside the chip opening. The chips are then placed in the incubator (37°C and 5% CO_2). The medium, containing Claycomb medium, 10% fetal bovine serum, 100U/ml-100µg/ml penicillin-streptomycin, 0.1mM norepinephrine, and 2mM L-glutamine, is exchanged every day and 2 hours before the measurements. The chips are kept in the incubator for 2-3 days, until the HL-1 cells form a confluent layer and start being electrically active.

C. Heart tissue preparation

The heart tissue was prepared by dissecting embryonic tissue E18 from a Wistar rat. The heart of an embryo is quickly isolated, washed in Hank's balanced salt solution (HBSS, Sigma, St. Louis, USA), then stored and measured in supplemented Claycomb medium.

The experiments are done with the approval of the Landesumweltamt für Natur, Umwelt und Verbraucherschutz Nordrhein-Westfalen, Recklinghausen, Germany, number 84-02.04.2015.A173.

D. Device characterization

As soon as fabricated and encapsulated, the devices are characterized by means of a Keithley 4200 SCS probe station. The drain – source potential (V_{DS}) is set to 50 mV or 100 mV, whereas the gate potential (V_{GS}) is swept against Ag/AgCl pellet electrode from 0 to 800 mV. A phosphate-buffered saline (PBS) solution of 150 mM salt concentration, and pH 7.4, was used as electrolyte to be as close to the physiological conditions as possible.

E. Noise measurements

The noise spectra are registered in the range from 1 Hz to 100 kHz using a measurement system, consisting of a low-noise pre-amplifier, developed in-house, an ITHACO amplifier and the Dynamic Signal Analyzer HP 35670A. The intrinsic input-referred thermal noises of the preamplifier and ITHACO amplifier were measured as 2×10^{-18} V^2Hz^{-1} and 2×10^{-17} V^2Hz^{-1}, respectively [19].

F. In-vitro time-series measurements

As soon as cells form a confluent layer on the chips, they are measured at a special multichannel measurements system. The multichannel set-up allows characterization (I-V) and parallel time series recordings of all 32 or 64 transistors per chip [20], [21]. The set-up consists of a pre-amplifier, which is mainly a GFET plus an operational amplifier. The choice of the feedback resistance (FBR) and the actual transconductane (g_m) of the operational point used results in the pre-amplification factor: $V_{out} = V_G \times g_m \times FBR$. Afterwards, the signal is passed to the main amplifier, which consists of several post-amplification stages. The FBR should be near or around the actual graphene channel's resistance for the best signal transfer. Prior to the time series measurements, I-V curves are recorded and further derived ($\Delta I_{DS}/\Delta V_{GS}$) in order to determine the highest transconductance point. Every further reported time-series recording is already recalculated fluctuations of the gate potential, $\Delta V_G = \frac{\Delta V_{out}}{g_m \times FBR}$ and adjusted to the cellular level.

G. PIonS and bending set-up

The bending is done at a mechanically controllable break junctions (MCBJ) set-up [22]. The steel substrate, supporting thin PI layer fits specifically to the break-junction. A conducting silver paste was manually applied to the gold feedlines and "drawn" further to increase the area and provide a reliable contact to conducting magnetic contacts. Polydimethylsiloxane (PDMS, Sylgard, mixture 40:1) is used

to create a ring to hold the liquid inside while bending and measuring for a long time.

The MCBJ set-up geometry allows the pushing rod to go a maximum of 5 mm upward (h_{max}=5 mm). Knowing the length (l) of the sample to be 37 mm, we can recalculate the maximum bending radius ($r = h/2 + l^2/8h$) to be 36.7 mm. The corresponding maximum tensile strain ($\varepsilon_0 = d/2r$), considering the sample thickness d=150μm, is approximately 0.2%.

III. Results and Discussion

A. Solution gating and sensitivity

While PIonS and SiO_2/Si devices are initially measured at the probe station in order to get the I-V characteristics, the sapphire devices were encapsulated and measured directly via the multichannel set-up. The behavior of our devices is similar to others, reported elsewhere [11], [23], [24]. Following the characterization, the I-V curves are derived in order to find the values of maximum transconductance. Notably, as usual for all of our devices, the holes conductivity and transconductance are usually slightly larger than that of electrons (data not shown). This feature is of special interest for further *in vivo* applications, since it allows us to work with V_{GS} potentials close to 0V.

However, transconductance obviously depends on the width to length ratio (W/L) of the gated graphene, which is seldom mentioned in the literature. The comprehensive design of our GFETs allows us to characterize devices with different lengths and widths and W/L ratios. The overall plot (Fig. 1) compares the values of our SiO_2/Si based GFETs (green oval), PIonS based GFETs (yellow oval), and sapphire based GFETs (purple point). Clearly visible is that increasing the width and decreasing the length of a device increases the overall transconductance. The best PIonS-based device shows a transconductance value of 11 mS·V^{-1} (1.1mS, V_{DS}=100mV, W=20 μm, L=3 μm, W/L=6.66), normalization to one square (one □ is when W/L=1, see inset of Fig. 1) results in 1.65 mS·V^{-1}·□. The device is shown with a black circle in Fig. 1. The linearized trend of the all working PIonS GFETs (number of evaluated transistors, n= 40) gives an average value of 1.9±0.9 mS·V^{-1}·□. This is the highest transconductance values of liquid-gated GFETs ever reported. Peculiarly, the flexible devices show distinct improvement of their behavior compared to the rigid devices, which can be explained by the inertness of the polyimide surface [12], [25] absence of dangling bonds and charge impurities, unlike in SiO_2/Si [26], [27], [28], [29].

The SiO_2/Si based GFETs (number of evaluated transistors, n=18) result in 630±580 μS·V^{-1}·□ normalized transconductance values. The large distribution of the values could be attributed to the dangling bonds of the silicon dioxide itself [27], making the fabrication of the GFETs on SiO_2/Si substrates less consistent than on sapphire or polyimide. This is the main problem with combining graphene and silicon technology, and the reason why we decided not to use the chips for further cellular measurements.

The sapphire substrates usually show better performance than SiO_2/Si, mostly due to high thermal conductivity and high energy of polar optical phonons, therefore the substrate-limited mobility is much higher than in SiO_2/Si [30]. The best reported [16] sapphire-based GFETs transconductance value is 2 mS·V^{-1}·□, as shown by the purple star in Fig. 1. At the same time, the sapphire-based devices used in this work, despite a long *in vitro* exposure of more than 10 cultures, up to 3 weeks long each, show an appropriate transconductance of 360±180 μS·V^{-1}·□ (number of evaluated transistors, n=105). Interestingly, we have not observed any toxicological effect due to a possible graphene parts being removed/starched by a cellular layer.

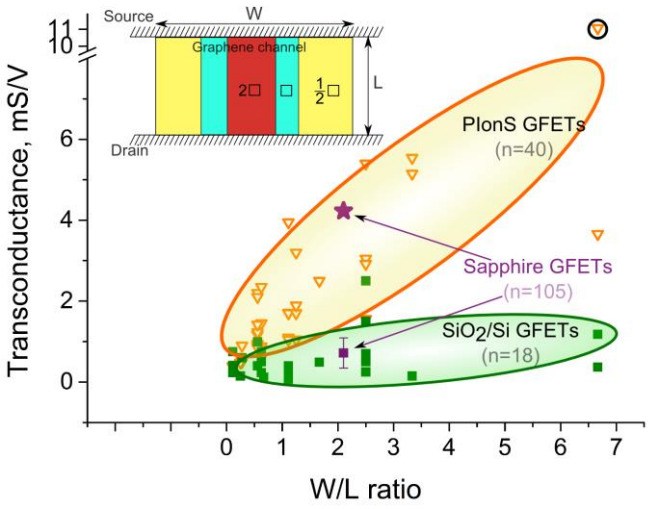

Fig. 1. A comparison plot of the voltage normalized transconductance distribution for GFETs of different W/L ratios and substrates. Yellow triangles and green squares represent the individual data points for each W/L ratio for PIonS and SiO_2/Si devices respectively. The semitransparent yellow and green ovals are given as eye guidelines to see the slopes. The purple square is the averaged data from sapphire-based devices from this work, whilst the purple star represents the data point for the best reported sapphire-based GFET [16]. The black circle shows the largest value of 11 mS·V^{-1} for a PIonS-based device. The inset is given for better understanding of the number of squares per graphene channel. The averaged relative maximum transconductance position (V_{GS}-V_D) is –150±50 mV. The V_{DS} potential applied during the measurements is 100 mV.

Mobilities of the devices are roughly estimated for the linear regimes of the I-V curves, considering the total interface capacitance of 2 μF/cm^2 - the capacitance value at the gate potential with maximum transconductance [23]. Similar to the transconductance behavior, the mobility is the highest for PIonS devices, and can reach 1750 cm^2·V^{-1}·s^{-1} for holes and 1200 cm^2·V^{-1}·s^{-1} for electrons. The usual mobility values of our sapphire GFETs are 1200 cm^2·V^{-1}·s^{-1} and 650 cm^2·V^{-1}·s^{-1} for holes and electrons, respectively. The SiO_2/Si based GFETs, as expected, show the lowest mobilities, in the range of 430 cm^2·V^{-1}·s^{-1} for holes and 300 cm^2·V^{-1}·s^{-1} for electrons. We would like to emphasize that these are the roughly estimated values, which could fluctuate considering the calculation model used and assumptions made therein. Nevertheless, the values show the above described trend of the transconductance values.

The overall large variations in device's performance can be related to (i) the surface contamination after the device fabrication steps; (ii) sometimes comparably low number of devices per each width and length.

As described above, for further cell measurements the most important values are transconductance (g_m) and noise.

Considering the read-out scheme of our multichannel measurement set-up, the pre-amplification factor is $g_m \times FBR$. Therefore, the higher the transconductance, the higher the pre-amplification. The second factor – the overall liquid gate noise is equally important and is analyzed in the following chapter.

B. *Noise analysis*

There are many different parameters which can be used to describe the noise of a system, including values of voltage spectral density (S_V), current spectral density (S_I) [31] or their normalized values (S_V/V^2 or S_I/I^2) [24], [32]. Here, we measure the S_I and S_I/I^2 noise spectra for PIonS and sapphire chips (see Fig. 2a and 2b). The values are still difficult to compare. Another, more reliable and comparable parameter is the effective gate noise, calculated similarly to [23] and plotted in Fig. 2d. The values, calculated for the frequency range from 1 Hz to 100 kHz, have a peak at the Dirac point due to the minima of the transconductance (Fig. 2d). In order to provide a correct comparison, the further noise values are taken from the point of maximum transconductance in the p-doping regime. As the noise performance depends on the device's active area, the following analysis is done only for the devices of almost the same area (200 µm^2 and 160 µm^2 for sapphire and PIonS GFETs correspondingly; unfortunately, due to large discrepancy of Si-based devices, we did not have a Si-based GFET with similar area). The position is marked as a star in the Fig. 2c and Fig 2d. The value is in the range of 40 µV for PIonS devices and 25 µV for sapphire devices. The best reported sapphire-based devices [16], [33] show the effective gate noise value of 12 µV at a similar relative gate potential, and graphene area (200 µm^2). We believe that the noise differences between the devices could be caused by the graphene's quality/transfer/fabrication differences, as well as by substrate's quality, i.e. density of charge impurities and traps [32], [34], [35], [36].

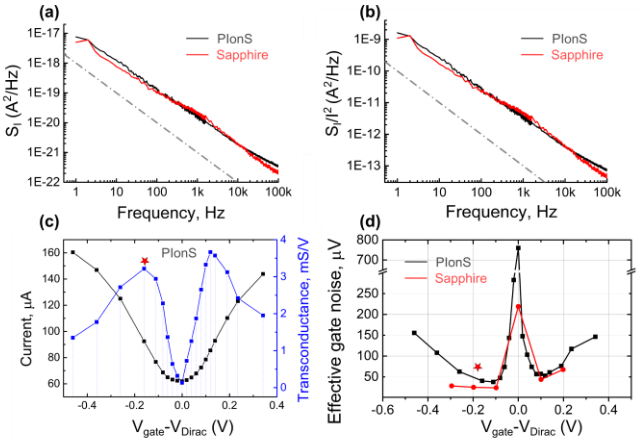

Fig. 2. The exemplary noise power spectral density S_I (a) and S_I/I^2 (b) plots for a PIonS device (in black), the I-V curve of which is in (c) and sapphire device (red). The spectra are taken at the V_{gate} position marked as star in (c) and (d). A gray dashed line is given as a 1/f guideline. In (d) is the plot of effective gate noise; black for PIonS device, red for sapphire device. The distinct peaks at the Dirac point position are due to transconductance minima and are also regularly noted in other works [23], [33]. W=20µm, L=10 µm for sapphire device and W=20µm, L=8 µm for the PIonS device. V_{Dirac} refers to the point of minimal current, i.e. Dirac point. The V_{DS} is always kept at 100mV for every measurement.

In view of the presented analysis, the sapphire-based GFETs were selected for use in *in vitro* tests. Optical transparency of the chips simplifies the soldering of the device to a chip carrier, and allows monitoring the progression of the cell culture as well, in order to select the best level of cell maturation for measurements. The PIonS chips, in contrary, are impossible to bond, encapsulate or observe culture progression.

C. *In-vitro recordings. Sapphire GFETs*

The *in vitro* measurements are done on the sapphire chips, which show comparably high transconductance values, and at the same time, low noise performance. HL-1 cell culture is chosen as the test cell culture, since the confluent cell layer leads to good cell-device coupling and APs are spontaneously generated by pacemaker cells. These APs are repetitive and propagate through the whole cellular layer [17], [37]. Furthermore, the associated cell contraction can be monitored to determine the maturity of the culture and therefore the appropriate time to measure electrical signals.The cells (Fig. 3a) are cultured on the encapsulated chip's surface (Fig. 3b) until they form a confluent layer. Usually this takes 2-3 days. As soon the cells reach confluency, and form gap junctions, they start beating, therefore producing the extracellular potentials. Considering that HL-1 cells form a syncytium, the signals propagate geometrically along the tissue. Pacemakers are the strongest cells in the culture, which create the rhythmic beatings for the whole monolayer. Thus, the HL-1 cellular layer is able to beat synchronously. Pacemaker cells play an important role when investigating HL-1 cells [38], [39]. Therefore, it is important to calculate not just the distinct action potentials, but their propagation. This is done via measuring all the devices per chip simultaneously via the specially fabricated multichannel measurement system (Fig. 3c) and controlled by the LabView-based software (Fig. 3d).

With the sapphire-based GFETs we have been able to record the cellular activity from several channels (devices) on a chip. Some of the time traces are plotted in Fig. 4a.[1] The timetraces represent the gate potential fluctuations, adjusted [40] to the cellular behavior, as described in section II.F of the manuscript. If zoomed into one of the APs (Fig. 4b), the time delay between different channels is visible. Which means that the signal is propagating through the cellular layer on top of the chip. Considering that over 10 channels per chip have recorded action

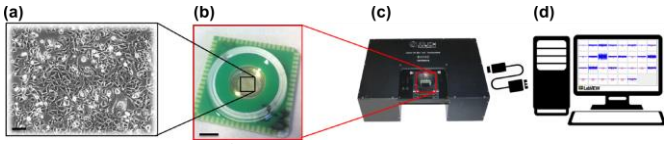

Fig. 3. The schematics of the *in vitro* experiments: (a) a transmitted light optical image of the HL-1 cell culture. Scale bar, 20 µm. (b) Photograph of the chip, bonded to the carrier and encapsulated by PDMS and glass rings for medium storage. Scale bar, 5 mm. (c) A multichannel measurement set-up, manipulated via PC (d) with Lab-View based software.

[1] 100Hz order 4 elliptic low pass zero phase filter is applied in order to simplify signal detection

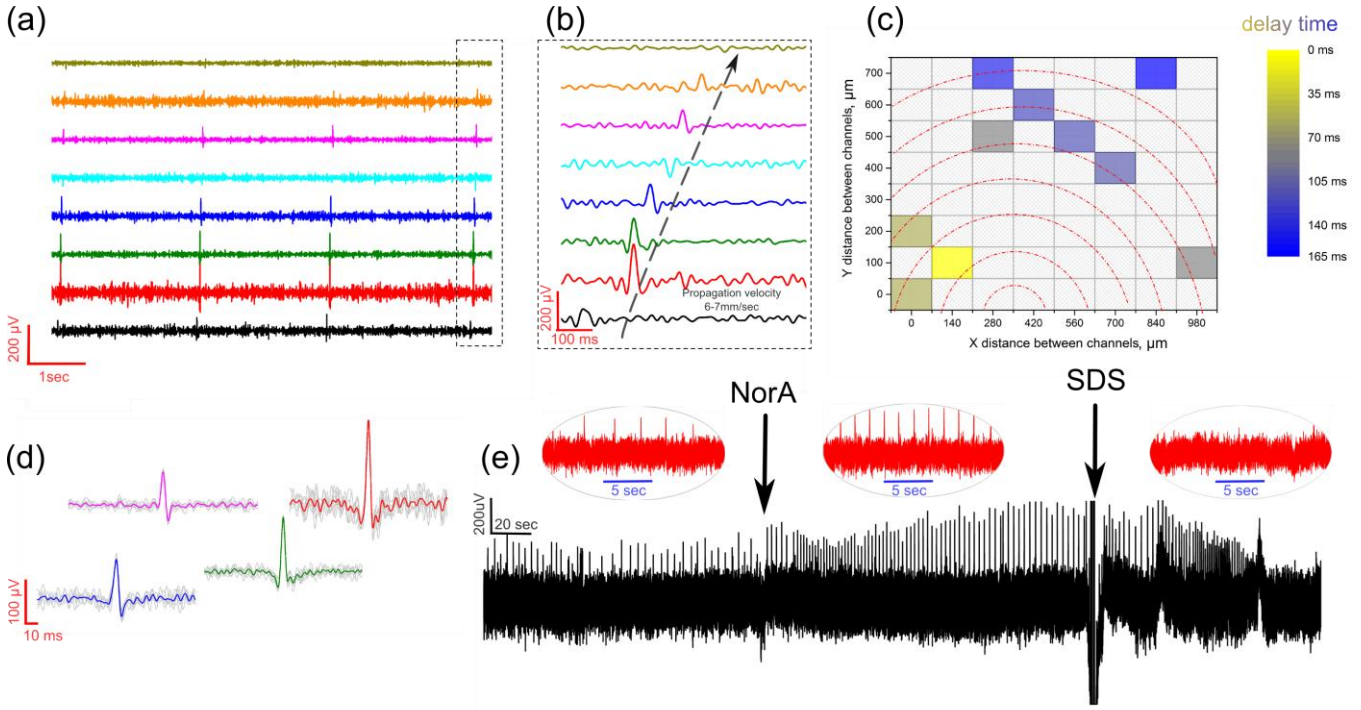

Fig. 4. The *in vitro* recordings from sapphire-based GFETs: (a) Eight seconds long time traces of 8 channels with recorded APs; operating point: V_{DS}=0.5V, V_{GS}=0.25V, hole region. (b) A zoom-in into one of the APs, signal delay between the channels means that signal propagates through the chip. (c) The heat plot of the signal propagation, considering the geometrical locations of the recorded channels. (d) APs from 4 different channels (correspondingly to red, green, blue and magenta time traces in Fig. 4a) are shown in gray with the averaged signal as an overlay. (e) Recording, over 10 minutes long, from another culture where initially APs are seen firing at a frequency of 0.3Hz (first inset), whereas addition of NorA into the culture medium almost doubles the frequency (>0.5Hz, second inset), and SDS starts to perforate and dissolve the cellular layer, decreasing the amplitude and eventually ceasing the APs (third inset). All three insets are 20 seconds long and have the same y-scale; operating point: V_{DS}=0.2V, V_{GS}=0.15V, hole region.

potentials, we calculated the spatial propagation of the signal (Fig. 4c). We extrapolated the pacemaker's location to the middle bottom of the chip. The signal propagates radially, which would be more visible if more working devices picked-up the signals. The calculated signal propagation velocity (upper bound) is estimated to be around 6-7 mm/sec, which is in satisfactory agreement with literature values [33], [41], [42].

The signal-to-noise ratio (SNR) of the recorded potentials varies from a GFET to a GFET and spans from 4 (the best one) to 1.5 (hardly visible). The noise is considered here and in the following as 2×standard deviation (SD). Shape and amplitude of a recorded action potentials are correlated to the expected extracellular potentials. In general, there are many parameters which can influence the extracellular potentials, such as sealing, cell-chip coupling, junction resistance, etc. [40], [43]. The differences in the SNR and in the signal shape (Fig. 4d) can be attributed to the difference in the transconductance values for different GFETs on a single chip, as described above, and the quality of sealing (cell-chip coupling) between a cell and a device [40].Whereas the first parameter can be controlled via a more robust and fault-free fabrication procedure, the second one can only be addressed with the type of cellular culture, surface treatment of the device for cell adhesion, etc [40], [43].

In order to prove the biological origin of the signals, another experiment with different setting parameters was performed on a similar sapphire-based GFET chip (Fig. 4e). While recording the time traces from the chip, norepinephrine (NorA), a well-known drug for heart rate stimulation, is added to the medium. Increase of the NorA concentration from 0.1 mM to 0.2-0.3 mM in the medium, doubles the beating frequency (Fig. 4e insets), as expected [44]. After that, a concentrated sodium dodecyl sulfate (SDS, a surfactant) solution was added to the same culture. The SDS perforates the cellular layer and removes it from the chip's surface. This results in frequent but evanescent beatings which disappear completely in a couple of minutes.

These experiments show that such devices fit perfectly into the field of *in vitro* measurements, drug-screening, and recording of action potential propagation, as described previously [29]. Nevertheless, the inflexibility of the substrate restricts us from performing *in vivo* tests. Flexible devices would be preferred for implantation into a body. The PIonS devices, present the same GFETs on a flexible polyimide that is supported on steel to ease handling in the lab. Future devices envision the GFETs on PI without any metal support. Therefore, the PIonS-based devices were further tested by measuring APs directly from *ex vivo* heart tissue.

D. Flexibility tests. PIonS GFETs

In order to test the reliability of the PIonS devices, we performed two kinds of the bending tests. The first test consisted of step-wise bending of the PIonS chip and concurrent measurement of the transfer curve at each bending angle (Fig. 5). After a step of 500 µm, we measure the device and then continue bending, consequently measuring after each step. We

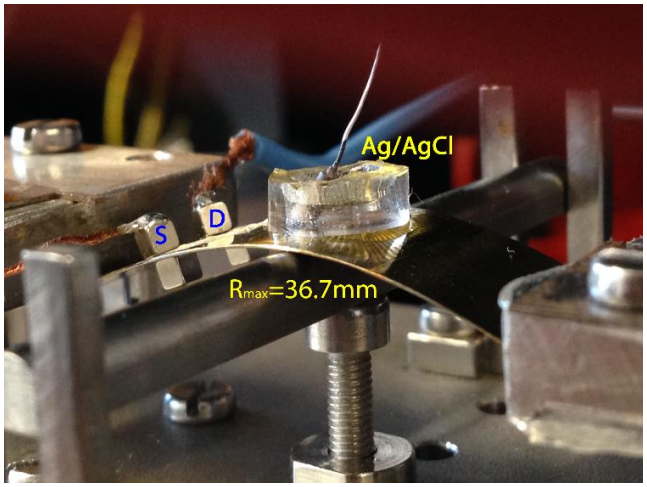

Fig 5. A picture of the bending set-up. The pushing rod is at its maximum height of 5mm and total bending radius of 36.7mm. S and D mark the conducting magnets, used for manual and stable connections while bending. PDMS ring works as the reservoir for the electrolyte solution, gated via Ag/AgCl pellet electrode.

found no significant changes in the R_D (resistance at the Dirac point) nor in the transconductance due to the bending (data not shown).

The second test was performed, continuously bending the chip for 10, 100, 300, and 1000 times up and down to the maximum tensile strain of 0.2%. The whole array of the GFETs is measured after each iteration. None of the GFETs, oriented perpendicular to the bending axis were broken or exhibited reduced performance. Nevertheless, some GFETs, oriented along the bending axis, got broken between the 300th and 1000th cycle. We speculate that this is the effect of the source-drain contacts to the graphene, since the tensile strain of 0.2% is not large enough to change internal properties of the graphene itself [45].

E. Ex-vivo recordings. PIonS GFETs

As an intermediate step towards *in vivo* measurements, we performed *ex vivo* recordings of embryonic rat heart tissue on a PIonS chip. The heart tissue was carefully placed directly in the middle of the chip (Fig. 6a), source and drain were connected as described in the experimental section. A Ag/AgCl pellet electrode is placed right on top of the tissue, and a large enough drop of electrolyte applied in order to transfer the gate potential, but small enough to not lift the tissue up from the surface.

The time series recordings, of almost two minutes long (Fig. 6b), show very remarkable peaks. The SNR of the measurement[2] is estimated around 10.5±0.5, considering the 930 µV noise (estimated as 2×SD) and the cellular signal amplitude of 9.75±0.5 mV. The amplitude of the heart tissue is much larger than of HL-1 cells, but we record local field potentials in this case, which are expected to be in this order [46], [47]. The peak's FWHM (Fig. 6c) is 6-7 ms which corresponds to the ion-channel current and not to the mechanical movement [47]. The extremely large noise values can be attributed to the suboptimal connections on the PIonS chips, necessary to allow both bending and *ex vivo* measurements. In order to provide noise values comparable to devices on stiff substrates, the same device was used for a dummy time series recording with more stable needle contacts, the result is plotted in red in Fig. 6b for comparison.

IV. Conclusion

In summary, three kinds of GFETs: on SiO_2/Si, sapphire, and PIonS substrates, were fabricated and investigated for their performance. Sapphire-based devices show uniformly stable transconductance values and low noise. The devices have been used for *in vitro* monitoring of cardiomyocyte activity and exhibit excellent SNR (up to 4 for HL-1 cells and 11 for *ex vivo* heart tissue). The controllably flexible PIonS GFETs exhibit an extremely large transconductance values, with average of 1.9±0.9 $mS \cdot V^{-1} \cdot \square$ and mobility as high as 1750 $cm^2 \cdot V^{-1} \cdot s^{-1}$. Bending tests and *ex vivo* measurements prove the reliability of the devices.

Releasing the underlying steel substrate would allow the devices to be easily implementable for *in vivo* applications. The combination of excellent transconductance values, combined

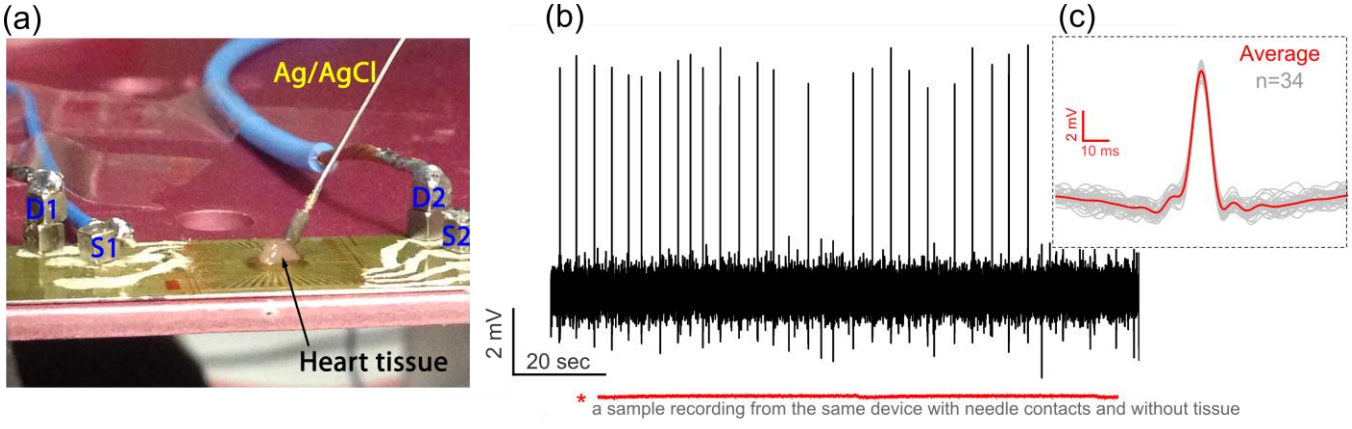

Fig. 6. (a) A photo of the *ex vivo* experiment on the flexible and controllably bendable GFETs chip, with heart tissue right on top of the chip. (b) The heart tissue measurement time trace; the red line is a time trace of the same device but with needle contacts and measured at the shielded setup used for the noise characterization, without heart tissue. (c) The averaged action potentials (n=34, in gray) from one recorded channel. Operating point: V_{DS}=0.15V, V_{GS}=0.25V, hole region.

[2] 10-100 Hz bandpass filter was applied to the recordings prior to analysis in order to reduce the environmental noise. Signal width of 15-20ms allows such filtering without losing useful information.

with considerably low noise level, open up the road for *in vivo* applications of the graphene-on-polyimide field effect transistors.

ACKNOWLEDGMENT

The authors would like to thank Sergii Pud, Wangyang Fu and Dirk Mayer for helpful discussions, Maristella Coppola for help with bending set-up and ICS-7 for the heart tissue preparation.

REFERENCES

[1] D. J. Bakkum, U. Frey, M. Radivojevic, T. L. Russell, J. Müller, M. Fiscella, H. Takahashi, and A. Hierlemann, "Tracking axonal action potential propagation on a high-density microelectrode array across hundreds of sites," *Nat. Commun.*, vol. 4, p. 2181, 2013.

[2] J. Rothe, O. Frey, A. Stettler, Y. Chen, and A. Hierlemann, "Fully integrated CMOS microsystem for electrochemical measurements on 32 × 32 working electrodes at 90 frames per second," *Anal. Chem.*, vol. 86, pp. 6425–6432, 2014.

[3] S. K. Arya, C. C. Wong, Y. J. Jeon, T. Bansal, and M. K. Park, "Advances in Complementary-Metal–Oxide–Semiconductor-Based Integrated Biosensor Arrays," *Chem. Rev.*, vol. 115, no. 11, pp. 5116–5158, 2015.

[4] P. Fattahi, G. Yang, G. Kim, and M. R. Abidian, "A review of organic and inorganic biomaterials for neural interfaces," *Adv. Mater.*, vol. 26, no. 12, pp. 1846–1885, 2014.

[5] M. HajjHassan, V. Chodavarapu, and S. Musallam, "NeuroMEMS: Neural probe microtechnologies," *Sensors*, vol. 8, no. 10, pp. 6704–6726, 2008.

[6] K. S. Novoselov, A K. Geim, S. V Morozov, D. Jiang, Y. Zhang, S. V Dubonos, I. V Grigorieva, and a a Firsov, "Electric field effect in atomically thin carbon films," *Science*, vol. 306, no. 5696, pp. 666–669, 2004.

[7] A. C. Ferrari, F. Bonaccorso, V. Fal'ko, K. S. Novoselov, S. Roche, P. Boggild, S. Borini, F. H. L. Koppens, V. Palermo, N. Pugno, J. A. Garrido, R. Sordan, A. Bianco, L. Ballerini, M. Prato, E. Lidorikis, J. Kivioja, C. Marinelli, T. Ryhanen, A. Morpurgo, J. N. Coleman, V. Nicolosi, L. Colombo, A. Fert, M. Garcia-Hernandez, A. Bachtold, G. F. Schneider, F. Guinea, C. Dekker, M. Barbone, Z. Sun, C. Galiotis, A. N. Grigorenko, G. Konstantatos, A. Kis, M. Katsnelson, L. Vandersypen, A. Loiseau, V. Morandi, D. Neumaier, E. Treossi, V. Pellegrini, M. Polini, A. Tredicucci, G. M. Williams, B. Hee Hong, J.-H. Ahn, J. Min Kim, H. Zirath, B. J. van Wees, H. van der Zant, L. Occhipinti, A. Di Matteo, I. A. Kinloch, T. Seyller, E. Quesnel, X. Feng, K. Teo, N. Rupesinghe, P. Hakonen, S. R. T. Neil, Q. Tannock, T. Lofwander, and J. Kinaret, "Science and technology roadmap for graphene{,} related two-dimensional crystals{,} and hybrid systems," *Nanoscale*, vol. 7, no. 11, pp. 4598–4810, 2015.

[8] A. Bendali, L. H. Hess, M. Seifert, V. Forster, A. Stephan, J. A Garrido, and S. Picaud, "Purified neurons can survive on peptide-free graphene layers," *Adv. Healthc. Mater.*, vol. 2, no. 7, pp. 929–33, 2013.

[9] F. Veliev, A. Briançon-Marjollet, V. Bouchiat, and C. Delacour, "Impact of crystalline quality on neuronal affinity of pristine graphene," *Biomaterials*, vol. 86, pp. 33–41, 2016.

[10] A. Fabbro, D. Scaini, V. León, E. Vázquez, G. Cellot, G. Privitera, L. Lombardi, F. Torrisi, F. Tomarchio, F. Bonaccorso, S. Bosi, A. C. Ferrari, L. Ballerini, and M. Prato, "Graphene-Based Interfaces Do Not Alter Target Nerve Cells," *ACS Nano*, vol. 10, no. 1, pp. 615–623, 2016.

[11] F. Chen, Q. Qing, J. Xia, J. Li, and N. Tao, "Electrochemical gate-controlled charge transport in graphene in ionic liquid and aqueous solution," *J. Am. Chem. Soc.*, vol. 131, no. 29, pp. 9908–9909, 2009.

[12] T. Stieglitz, H. Beutel, M. Schuettler, and J.-U. Meyer, "Micromachined, Polyimide-Based Devices for Flexible Neural Interfaces," *Biomed. Microdevices*, vol. 2, no. 4, pp. 283–294, 2000.

[13] T. Wu, X. Zhang, Q. Yuan, J. Xue, G. Lu, Z. Liu, H. Wang, H. Wang, F. Ding, Q. Yu, X. Xie, and M. Jiang, "Fast growth of inch-sized single-crystalline graphene from a controlled single nucleus on Cu-Ni alloys," *Nat. Mater.*, vol. 15, no. 1, pp. 43–47, 2015.

[14] G. Borin Barin, Y. Song, I. de Fátima Gimenez, A. G. Souza Filho, L. S. Barreto, and J. Kong, "Optimized graphene transfer: Influence of polymethylmethacrylate (PMMA) layer concentration and baking time on graphene final performance," *Carbon*, vol. 84, pp. 82–90, 2015.

[15] B. M. Blaschke, M. Lottner, S. Drieschner, A. B. Calia, K. Stoiber, L. Rousseau, G. Lissourges, and J. A. Garrido, "Flexible graphene transistors for recording cell action potentials," *2D Mater.*, vol. 3, no. 2, p. 025007, 2016.

[16] L. H. Hess, M. V. Hauf, M. Seifert, F. Speck, T. Seyller, M. Stutzmann, I. D. Sharp, and J. A. Garrido, "High-transconductance graphene solution-gated field effect transistors," *Appl. Phys. Lett.*, vol. 99, no. 3, p. 033503, 2011.

[17] W. C. Claycomb, N. A. Lanson, B. S. Stallworth, D. B. Egeland, J. B. Delcarpio, A. Bahinski, and N. J. Izzo, "HL-1 cells: a cardiac muscle cell line that contracts and retains phenotypic characteristics of the adult cardiomyocyte," *Proc. Natl. Acad. Sci. U. S. A.*, vol. 95, no. 6, pp. 2979–2984, 1998.

[18] L. Sartiani, P. Bochet, E. Cerbai, A. Mugelli, and R. Fischmeister, "Functional expression of the hyperpolarization-activated, non-selective cation current I f in immortalized HL-1 cardiomyocytes," *J. Physiol.*, vol. 545, no. 1, pp. 81–92, 2002.

[19] S. A. Vitusevich, S. V. Danylyuk, N. Klein, M. V. Petrychuk, V. N. Sokolov, V. A. Kochelap, A. E. Belyaev, V. Tilak, J. Smart, A. Vertiatchikh, and L. F. Eastman, "Excess low-frequency noise in AlGaN/GaN-based high-electron-mobility transistors," *Appl. Phys. Lett.*, vol. 80, no. 12, p. 2126, 2002.

[20] M. Jansen, "Silizium Nanoribbon Feld-Effekt Transistoren zur Kopplung an elektroaktive Zellen," PhD dissertation, RWTH Aachen, Aachen, Germany, 2012.

[21] T. Qiu, et al., "A 64-Channel System based on Source-Follower for Extracellular Action Potential Measurement with Field-Effect-Transistor Sensors," to be published.

[22] D. Xiang, H. Jeong, T. Lee, and D. Mayer, "Mechanically controllable break junctions for molecular electronics," *Adv. Mater.*, vol. 25, no. 35, pp. 4845–4867, 2013.

[23] M. Dankerl, M. V. Hauf, A. Lippert, L. H. Hess, S. Birner, I. D. Sharp, A. Mahmood, P. Mallet, J.-Y. Veuillen, M. Stutzmann, and J. A. Garrido, "Graphene Solution-Gated Field-Effect Transistor Array for Sensing Applications," *Adv. Funct. Mater.*, vol. 20, no. 18, pp. 3117–3124, 2010.

[24] Z. Cheng, J. Hou, Q. Zhou, T. Li, H. Li, L. Yang, K. Jiang, C. Wang, Y. Li, and Y. Fang, "Sensitivity limits and scaling of bioelectronic graphene transducers.," *Nano Lett.*, vol. 13, no. 6, pp. 2902–2907, 2013.

[25] M. Ghosh, "Polyimides: Fundamentals and Applications" Taylor & Francis, 1996.

[26] B. Guo, L. Fang, B. Zhang, and J. R. Gong, "Graphene Doping: A Review," *Insciences J.*, vol. 1, no. 2, pp. 80–89,. 2011.

[27] S. Fratini and F. Guinea, "Substrate-limited electron dynamics in graphene," *Phys. Rev. B*, vol. 77, no. 19, p. 195415, 2008.

[28] C. Jang, S. Xiao, M. Ishigami, and M. S. Fuhrer, "Intrinsic and extrinsic performance limits of graphene devices on SiO_2," *Nat. Nanotechnol.*, vol. 3, no. 4, pp. 206–209, 2008.

[29] E. H. Hwang, S. Adam, and S. Das Sarma, "Carrier transport in two-dimensional graphene layers," *Phys. Rev. Lett.*, vol. 98, no. 18, pp. 2–5, 2007.

[30] E. Pallecchi, C. Benz, A. C. Betz, H. v. Löhneysen, B. Plaçais, and R. Danneau, "Graphene microwave transistors on sapphire substrates," *Appl. Phys. Lett.*, vol. 99, no. 11, p. 113502, 2011.

[31] J. Cheng, L. Wu, X.-W. Du, Q.-H. Jin, J.-L. Zhao, and Y.-S. Xu, "Flexible Solution-Gated Graphene Field Effect Transistor for Electrophysiological Recording," *J. Microelectromechanical Syst.*, vol. 23, no. 6, pp. 1311–1317, 2014.

[32] Y. Zhang, E. E. Mendez, and X. Du, "Mobility-dependent low-frequency noise in graphene field-effect transistors," *ACS Nano*, vol. 5, no. 10, pp. 8124–8130, 2011.

[33] L. H. Hess, M. Jansen, V. Maybeck, M. V Hauf, M. Seifert, M. Stutzmann, I. D. Sharp, A. Offenhäusser, and J. a Garrido, "Graphene transistor arrays for recording action potentials from electrogenic cells," *Adv. Mater.*, vol. 23, no. 43, pp. 5045–5049, 4968, 2011.

[34] Z. Cheng, Q. Li, Z. Li, Q. Zhou, and Y. Fang, "Suspended Graphene Sensors with Improved Signal and Reduced Noise," *Nano Lett.*, vol. 10, no. 5, pp. 1864-1868, 2010.

[35] M. Kayyalha, and Y. P. Chen, "Observation of reduced 1/f noise in graphene field effect transistors on boron nitride substrates," *Appl. Phys. Lett.*, vol. 107, p. 113101, 2015.

[36] I. Heller, S. Chatoor, J. Männik, M. A. G. Zevenbergen, J. B. Oostinga, A. F. Morpurgo, C. Dekker, and S. G. Lemay, "Charge Noise in Graphene Transistors," *Nano Letters*, vol. 10, no.5, pp. 1563-1567, 2010.

[37] S. M. White, P. E. Constantin, and W. C. Claycomb, "Cardiac physiology at the cellular level: use of cultured HL-1 cardiomyocytes for studies of

cardiac muscle cell structure and function," *Am. J. Physiol. Heart Circ. Physiol.*, vol. 286, no. 3, pp. H823–H829, 2004.

[38] J. P. Fahrenbach, R. Mejia-Alvarez, and K. Banach, 2007, "The relevance of non-excitable cells for cardiac pacemaker function," *J Physiol*, vol. 585, pp. 565–578, 2007.

[39] Z. Yang and K. T. Murray, "Ionic Mechanisms of Pacemaker Activity in Spontaneously-contracting Atrial HL-1 Cells," *J. Cardiovasc. Pharmacol.*, vol. 57, no. 1, pp. 28–36, 2011.

[40] P. Fromherz, "Extracellular recording with transistors and the distribution of ionic conductances in a cell membrane," *Eur. Biophys. J.*, vol. 28, pp. 254–258, 1999.

[41] V. Maybeck, R. Edgington, A. Bongrain, J. O. Welch, E. Scorsone, P. Bergonzo, R. B. Jackman, and A. Offenhäusser, "Boron-Doped Nanocrystalline Diamond Microelectrode Arrays Monitor Cardiac Action Potentials," *Adv. Healthc. Mater.*, vol. 3, no. 2, pp. 283–289, 2014.

[42] B. Hofmann, V. Maybeck, S. Eick, S. Meffert, S. Ingebrandt, P. Wood, E. Bamberg, and A. Offenhäusser, "Light induced stimulation and delay of cardiac activity," *Lab on a Chip*, vol. 10, no. 19, pp. 2588–2596, 2010.

[43] M. Schottdorf, B. Hofmann, E. Kätelhön, A. Offenhäusser, and B. Wolfrum, "Frequency-dependent signal transfer at the interface between electrogenic cells and nanocavity electrodes," *Phys. Rev. E*, vol. 85, no. 3, p. 031917, 2012.

[44] A. R. Natarajan, Q. Rong, A. N. Katchman, and S. N. Ebert, "Intrinsic cardiac catecholamines help maintain beating activity in neonatal rat cardiomyocyte cultures," *Pediatr. Res.*, vol. 56, no. 3, pp. 411–7, 2004.

[45] B. K. Sharma and J.-H. Ahn, "Graphene based field effect transistors: Efforts made towards flexible electronics," *Solid. State. Electron.*, vol. 89, pp. 177–188, 2013.

[46] A. Stett, U. Egert, E. Guenther, F. Hofmann, T. Meyer, W. Nisch, and H. Haemmerle, "Biological application of microelectrode arrays in drug discovery and basic research," *Anal. Bioanal. Chem.*, vol. 377, no. 3, pp. 486–495, 2003.

[47] B. P. Timko, T. Cohen-Karni, G. Yu, Q. Qing, B. Tian, and C. M. Lieber, "Electrical Recording from Hearts with Flexible Nanowire Device Arrays," *Nano Lett.*, vol. 9, no. 2, pp. 914–918, 2009.